Electronic Supplementary Material (ESI) for Nanoscale Advances.

Supporting Information: Multifunctional Metasails for Self-stabilized Beam-riding and Optical Communication

Mohammad Rasoul Taghavi, Mohammad Mahdi Salary, and Hossein Mosallaei

September 12, 2021

The Supporting Information is organized into two sections:

S1. Further Details on the Modeling Approach,

S2. Full-Wave Simulation of the Geometric Phase Arrays.

S1. Further Discussion on Modeling Procedure

In this section, we outline more details regarding the approach used for modeling the optomechanical response of large-area metasails and obtain the closed-form expressions for the optical force components imparted to the metasail. The local optical force imparted to a group of unit cells across the metasail can be obtained by evaluating the flux of Maxwell's stress tensor through a box enclosing the group of unit cells. Given that the dominant contribution to the force results from the front and back surfaces of the enclosing box being parallel to the plane of metasail $(x-y)$, the time-averaged local force can be written as:

$$\langle \overrightarrow{dF} \rangle = \frac{1}{2} Re\{\hat{n}_i . \overline{\overline{T}}_{\text{em}} + \hat{n}_t . \overline{\overline{T}}_{\text{em}}\} dS \tag{1}$$

in which $\hat{n}_i$ and $\hat{n}_t$ are the surface normal vectors for the illumination side and transmission side, respectively, and $\overline{\overline{T}}_{\rm em}$ is Maxwell's stress tensor which is given by:

$$\overline{\overline{T}}_{\rm em} = \overrightarrow{D}\overrightarrow{E} + \overrightarrow{B}\overrightarrow{H} - \frac{1}{2}\overline{\overline{I}}_{3\times 3}(\overrightarrow{D}.\overrightarrow{E} + \overrightarrow{B}.\overrightarrow{H}) \tag{2}$$

where $\overrightarrow{D}, \overrightarrow{E}, \overrightarrow{B}$ and $\overrightarrow{H}$ are the electric displacement, electric and magnetic induction and magnetic field vectors, respectively, and $\overline{\overline{I}}_{3\times 3}$ is a unity dyad.

Assuming that incident field is a left-handed circularly polarized beam and decomposing the total fields into incident, reflected and transmitted fields, the local force can also be decomposed into the contribution of incident, reflected and transmitted fields as $\langle\overrightarrow{dF}\rangle = \langle\overrightarrow{dF_i}\rangle + \langle\overrightarrow{dF_r}\rangle + \langle\overrightarrow{dF_t}\rangle$ which can be obtained as the following by taking into account the contributions of co- and cross-polarized scattering:

$$\begin{aligned}\langle\overrightarrow{dF_i}\rangle = &\frac{\hat{z}}{2}\epsilon_0|E_i(x,y)|^2\cos^2(\theta_i)dS \\ &+ \frac{\hat{x}}{2}\epsilon_0|E_i(x,y)|^2\cos\theta_i\sin\theta_i\cos\varphi_i dS \\ &+ \frac{\hat{y}}{2}\epsilon_0|E_i(x,y)|^2\cos\theta_i\sin\theta_i\sin\varphi_i dS\end{aligned} \tag{3}$$

$$\begin{aligned}\langle\overrightarrow{dF_r}\rangle = &\frac{\hat{z}}{2}\epsilon_0|E_i(x,y)|^2|r_{\rm LL}(x,y,\lambda,\theta_i,\varphi_i)|^2\cos^2(\theta_{r\rm LL})dS \\ &+ \frac{\hat{z}}{2}\epsilon_0|E_i(x,y)|^2|r_{\rm LR}(x,y,\lambda,\theta_i,\varphi_i)|^2\cos^2(\theta_{r\rm LR})dS \\ &- \frac{\hat{x}}{2}\epsilon_0|E_i(x,y)|^2|r_{\rm LL}(x,y,\lambda,\theta_i,\varphi_i)|^2\cos(\theta_{r\rm LL})\sin(\theta_{r\rm LL})\cos(\varphi_{r\rm LL})dS \\ &- \frac{\hat{x}}{2}\epsilon_0|E_i(x,y)|^2|r_{\rm LR}(x,y,\lambda,\theta_i,\varphi_i)|^2\cos(\theta_{r\rm LR})\sin(\theta_{r\rm LR})\cos(\varphi_{r\rm LR})dS \\ &- \frac{\hat{y}}{2}\epsilon_0|E_i(x,y)|^2|r_{\rm LL}(x,y,\lambda,\theta_i,\varphi_i)|^2\cos(\theta_{r\rm LL})\sin(\theta_{r\rm LL})\sin(\varphi_{r\rm LL})dS \\ &- \frac{\hat{y}}{2}\epsilon_0|E_i(x,y)|^2|r_{\rm LR}(x,y,\lambda,\theta_i,\varphi_i)|^2\cos(\theta_{r\rm LR})\sin(\theta_{r\rm LR})\sin(\varphi_{r\rm LR})dS\end{aligned} \tag{4}$$

$$
\begin{aligned}
\langle\overrightarrow{dF_t}\rangle = & -\frac{\hat{z}}{2}\epsilon_0|E_i(x,y)|^2|t_{\mathrm{LL}}(x,y,\lambda,\theta_i,\varphi_i)|^2\cos^2(\theta_{t\mathrm{LL}})dS \\
& -\frac{\hat{z}}{2}\epsilon_0|E_i(x,y)|^2|t_{\mathrm{LR}}(x,y,\lambda,\theta_i,\varphi_i)|^2\cos^2(\theta_{t\mathrm{LR}})dS \\
& -\frac{\hat{x}}{2}\epsilon_0|E_i(x,y)|^2|t_{\mathrm{LL}}(x,y,\lambda,\theta_i,\varphi_i)|^2\cos(\theta_{t\mathrm{LL}})\sin(\theta_{t\mathrm{LL}})\cos(\varphi_{t\mathrm{LL}})dS \\
& -\frac{\hat{x}}{2}\epsilon_0|E_i(x,y)|^2|t_{\mathrm{LR}}(x,y,\lambda,\theta_i,\varphi_i)|^2\cos(\theta_{t\mathrm{LR}})\sin(\theta_{t\mathrm{LR}})\cos(\varphi_{t\mathrm{LR}})dS \\
& -\frac{\hat{y}}{2}\epsilon_0|E_i(x,y)|^2|t_{\mathrm{LL}}(x,y,\lambda,\theta_i,\varphi_i)|^2\cos(\theta_{t\mathrm{LL}})\sin(\theta_{t\mathrm{LL}})\sin(\varphi_{t\mathrm{LL}})dS \\
& -\frac{\hat{y}}{2}\epsilon_0|E_i(x,y)|^2|t_{\mathrm{LR}}(x,y,\lambda,\theta_i,\varphi_i)|^2\cos(\theta_{t\mathrm{LR}})\sin(\theta_{t\mathrm{LR}})\sin(\varphi_{t\mathrm{LR}})dS
\end{aligned}
\tag{5}
$$

wherein r_{LL} and t_{LL} are the reflection and transmission coefficients corresponding to the left-handed circularly polarized scattered beams under illumination of a left-handed circularly polarized beam, r_{LR} and t_{LR} are the reflection and transmission coefficients corresponding to the right-handed circularly polarized scattered beams under illumination of a left-handed circularly polarized beam, θ_i and φ_i are the polar and azimuthal angles of incidence, $\theta_{r\mathrm{LL}}$ and $\varphi_{r\mathrm{LL}}$ are the polar and azimuthal angles of reflection for the left-handed circularly polarized beam under illumination of a left-handed circularly polarized light, and $\theta_{r\mathrm{LR}}$ and $\varphi_{r\mathrm{LR}}$ are the polar and azimuthal angles of reflection for the right-handed circularly polarized beam under illumination of a left-handed circularly polarized light. $\theta_{t\mathrm{LL}}$, $\varphi_{t\mathrm{LL}}$, $\theta_{t\mathrm{LR}}$, and $\varphi_{t\mathrm{LR}}$ denote the same for the transmitted beams. The reflection and transmission angles are obtained based on generalized Snell's laws according to the spatial phase gradient profiles (Φ) imparted to the wavefronts of scattered light as the following:

$$
\sin(\theta_{r_{LL}})\cos(\varphi_{r_{LL}}) = -\frac{1}{k_0}\frac{\partial\Phi_{r_{LL}}(x,y)}{\partial_x} + \sin(\theta_i)\cos(\varphi_i) \tag{6}
$$

$$
\sin(\theta_{r_{LL}})\sin(\varphi_{r_{LL}}) = -\frac{1}{k_0}\frac{\partial\Phi_{r_{LL}}(x,y)}{\partial_y} + \sin(\theta_i)\sin(\varphi_i) \tag{7}
$$

$$
\sin(\theta_{t_{LR}})\cos(\varphi_{t_{LR}}) = -\frac{1}{k_0}\frac{\partial\Phi_{t_{LR}}(x,y)}{\partial_x} + \sin(\theta_i)\cos(\varphi_i) \tag{8}
$$

$$
\sin(\theta_{t_{LR}})\sin(\varphi_{t_{LR}}) = -\frac{1}{k_0}\frac{\partial\Phi_{t_{LR}}(x,y)}{\partial_y} + \sin(\theta_i)\sin(\varphi_i) \tag{9}
$$

In the above equations, the subscripts LL and LR denote the quantities corresponding to the left-handed and right-handed circularly polarized beams under illumination of

a left-handed circularly polarized incident beam, and the subscripts r and t stand for reflected and transmitted beams. It should be noted that the partial derivative of Φ_{rLR} and Φ_{tLL} with respect to spatial coordinates are zero given that only the scattered light undergone cross circular polarization conversion experiences the geometric phase. As a result, θ_{rLR}, φ_{rLR}, θ_{tLL}, and φ_{tLL} are ordinary reflection and transmission angles while the rest of the angles are anomalous angles. The geometric phase spatial profiles of Φ_{rLL} and Φ_{tLR} are determined by the orientation of unit cells across the interleaved metasail under the assumption of local periodicity which are set to yield parabolic phase profiles with different focal distances for propulsion and communication sub-arrays at the wavelength of propulsion laser and communication, as described in the manuscript. Using Eqs. (3)-(9) and full-wave RCWA simulation of unit cells in periodic arrangement, one can obtain the imparted optical forces to the sail for any given nanostructured geometry of the metasail under the assumption of local periodicity.

S2. Full-wave Simulations

As noted in the previous section and in the main manuscript, the optomechanical response of the large-area metasail is evaluated by modeling the optical response based on generalized Snell's law under the assumption of local periodicity. This choice has been made due to the fact that metasail dimensions extend over many wavelengths of light while featuring subwavelength unit cells which rules out the possibility of a full-wave simulation due to enormous computational complexity. Here, we conduct a full-wave simulation of supercells consisting a periodic arrangement of a group of unit cells using rigorous coupled wave analysis (RCWA) to verify the broadband wavefront engineering capability of the designed unit cells for propulsion and communication sub-arrays, and evaluate agreement of the optical responses with the predictions of the generalized Snell's law based on local periodicity. For this purpose, we consider a periodic arrangement of two supercells formed by propulsion and communication unit cells as shown in Fig. 1(a) and (b), respectively. Both supercells are consisted of six unit cells along x axis whose orientations are set such that the reflected light undergone cross circular polarization conversion (E_{LL}) is steered

toward $\theta_{r\mathrm{LL}} = 18^\circ$ at $\lambda_0 = 1.3$ μm for the propulsion array and toward $\theta_{r\mathrm{LL}} = 15^\circ$ at $\lambda_\mathrm{c} = 1065$ nm for the communication array. Figure 1(c) shows the results of simulations for the wavefront of reflected light undergone cross circular polarization conversion. The sub-figures showing the results in the wavelength range of $\lambda = 1300$ nm - $\lambda = 1600$ nm correspond to the supercell of propulsion unit cells while the subfigure showing the result at $\lambda = 1065$ nm corresponds to the supercell of communication unit cells. As it can be clearly observed from the results, the reflected wavefronts are steered toward anomalous reflection angles in the account of experiencing geometric phase. Minimal spurious scattering is observed for the reflected light from the supercell of propulsion unit cells indicating uniformity of reflection across the array while the anomalous reflection response persists in a broad bandwidth due to dispersionless property of geometric phase. The direction of reflected wavefront at $\lambda_0 = 1.3$ μm denoted by the white arrow points toward $\theta_{r\mathrm{LL}} = 18^\circ$ which is in excellent agreement with the prediction of generalized Snell's law under assumption of local periodicity. Moreover, the reflection angle grows steeper at longer wavelengths due to dispersive response of the array which is consistent with prescription of Eqs. (6)-(7). For the supercell consisting of communication unit cells at $\lambda_c = 1065$ nm, although the spurious scattering is more considerable due to non-negligible coupling effects between adjacent unit cells, the reflection response is dominated by the anomalous reflection and the wavefront is mainly pointing toward $\theta_{r\mathrm{LL}} = 15^\circ$ as denoted by the white arrow. It is noteworthy to mention that the sail's aperture is divided into few sections and still each section has a very large dimension with respect to the operating wavelength. Considering the assured applicability of the local periodicity, optical functionality of each subsection is independent of the neighbouring subsections although around the edges local periodicity assumption may not be satisfied well, but they are very small fraction of the whole array. Consequently the utilized approximate method for applied force calculation is in good agreement with the full-wave simulation results.

The results included in this section point toward applicability of the generalized Snell's law based on local periodicity assumption to describe the optical response of large-area metasails and bring out the essential physics of the optomechanical response.

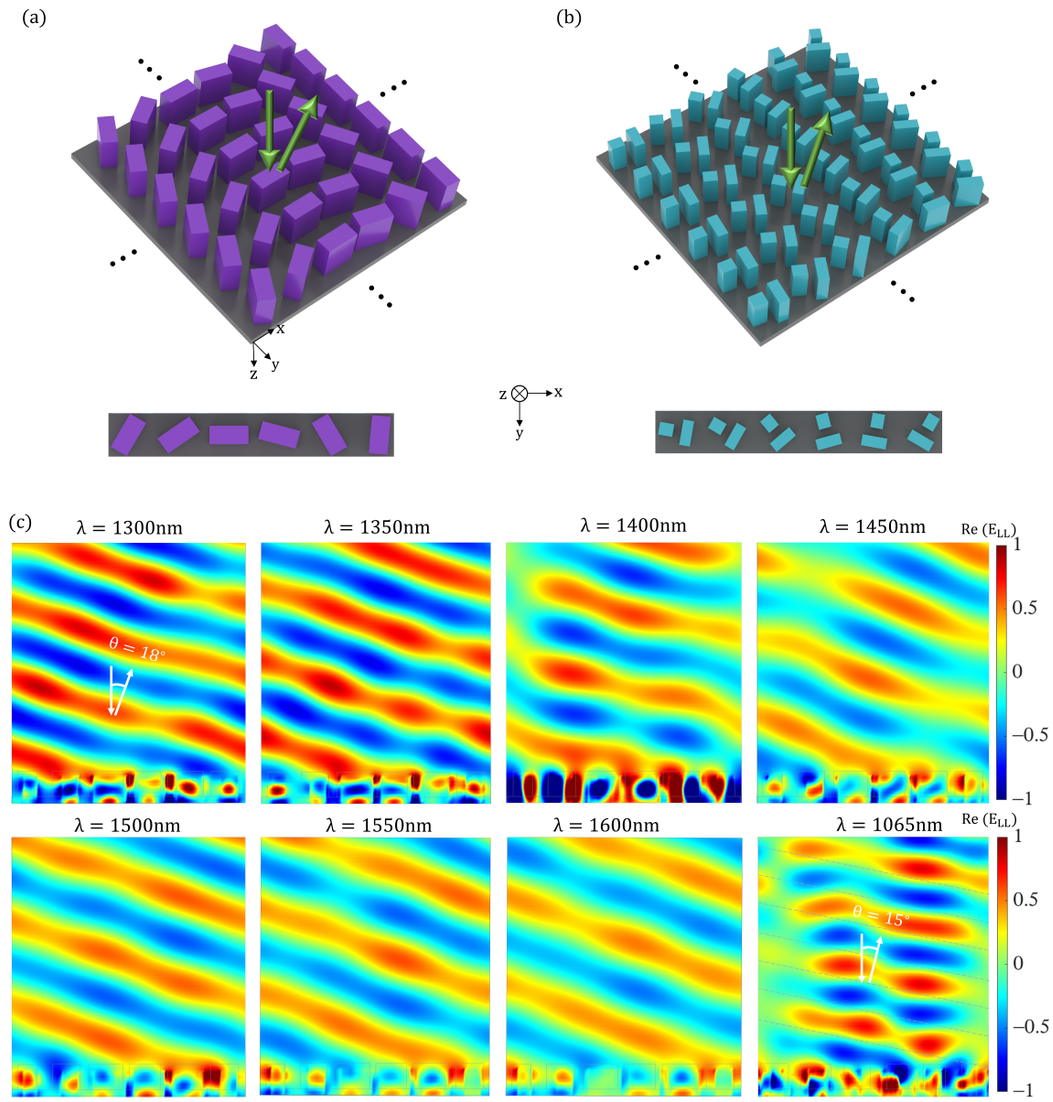

Figure 1: Depiction of supercells consisting of (a) six propulsion unit cells and (b) six communication unit cells whose orientations are set to steer the reflected light undergone cross circular polarization conversion toward $\theta_{r\mathrm{LL}} = 18°$ and $\theta_{r\mathrm{LL}} = 15°$, respectively. (c) The full-wave RCWA simulation results for the wavefronts of reflected light undergone cross circular polarization conversion. The wavefronts shown in the wavelength range of λ = 1300 nm - λ = 1600 nm correspond to the supercell of propulsion unit cells while the subfigure showing the result at λ = 1065 nm corresponds to the supercell of communication unit cells.